PROCEEDINGS, Thirty-Fifth Workshop on Geothermal Reservoir Engineering
Stanford University, Stanford, California, February 1-3, 2010
SGP-TR-188

ROCK MECHANICAL TESTING AND PETROLOGIC ANALYSIS IN SUPPORT OF WELL STIMULATION ACTIVITIES AT THE DESERT PEAK GEOTHERMAL FIELD, NEVADA

Susan Juch Lutz[1], Stephen Hickman[2], Nicholas Davatzes[3], Ezra Zemach[4], Peter Drakos[4], and Ann Robertson-Tait[5]

1 TerraTek, A Schlumberger Company, Salt Lake City, UT 84104
2 U.S. Geological Survey, Menlo Park, CA 94025
3 Temple University, Philadelphia, PA 19122
4 ORMAT Nevada Inc., Reno NV 89511-1136
5 GeothermEx Inc., Richmond, CA 94806
e-mail: slutz@salt-lake-city.oilfield.slb.com

ABSTRACT

In preparation for well stimulation activities and the development of an enhanced geothermal system (EGS) in the Desert Peak geothermal field, a series of petrologic and rock mechanical tests were conducted on selected core samples to represent the proposed stimulation interval within Well 27-15. The stimulation interval (3000-3500 ft; 930-1085 m) consists of Tertiary rhyolite tuffs that overlie metamorphic basement rocks consisting of siliceous argillite and other fractured metasedimentary rocks. Petrographic and X-ray diffraction mineralogic analyses indicate that the rhyolitic rocks are variably devitrified, argillaceous, and siliceous; and host minor amounts of quartz-dolomite-calcite veins in siliceous units along the basement contact. Hydrothermal clays are dominated by expandable smectite-rich mixed-layer illite-smectite.

Deeper in the metamorphic basement, young fractures are only partially mineralized with dolomite, siderite, calcite, and barite. The latter represent lightly permeable open fractures identified by a suite of acoustic and electrical image logs and and pressure-temperature-spinner flowmeter surveys collected in this interval of the well. Hydraulic stimulation of the well is intended to enhance formation permeability through self-propping shear failure along the most optimally oriented and critically stressed of these fractures.

Rock mechanical testing was conducted on the core samples to determine mechanical properties of the various lithologies including: radial versus axial volumetric strain, stress-strain relationships, dynamic versus static Young's moduli, and frictional strengths and failure responses under a variety of confining conditions. The results of the laboratory tests were used to construct Mohr-Coulomb failure envelopes for the proposed reservoir rocks. Pre- and post- test measurements on the deformed core plugs indicate up to a 20-fold enhancement in permeability in the originally tight rhyolite units as a result of shearing. Assuming that failure occurs on the same structural features in the well as in the core, these laboratory studies directly test the shear dilation concept in these clay-rich rocks, and are being used in combination with borehole stress measurements and fracture logging to predict fluid pressures required for initiation of shear dilation and permeability development within the geothermal reservoir.

INTRODUCTION

Petrologic evaluation was conducted on selected core and well cuttings samples collected from two drillholes in the Desert Peak geothermal field in northwestern Churchill County, Nevada (Figure 1). The purpose of this work is to describe petrologic characteristics of rocks within the proposed stimulation interval of Well 27-15 (Figure 2) that can be related to the geomechanical character and fracturing potential of these stratigraphic units where ambient temperatures are ~180 to 195° C. Mechanical testing of analogous core samples from nearby well 35-13 was also conducted in preparation for mechanical and chemical stimulation of Well 27-15, as part of DOE-Ormat's Enhanced Geothermal System (EGS) Project.

METHODS

The proposed stimulation interval within Well 27-15 consists of variably clayey to silicified Tertiary rhyolite ash flow tuffs that overlie weakly metamorphosed mudstones in the pre-Tertiary basement. Petrographic and mineralogic analyses were conducted on well cuttings samples from 27-15 that represent the stimulation interval (3000-3500 ft). Similar lithologies are represented by core samples collected from Well 35-13 (see Figure 1) in the depth

interval from 2276 ft to 2742 ft. Mechanical testing of these core samples was conducted at TerraTek.

Petrologic Analyses

The lithologies, composition, texture, vein and secondary mineralogy of the represented rock units in both 27-15 and 35-13 are based on thin section examination, with semi-quantitative X-ray diffraction (XRD) analysis on matching samples to better constrain rock mineralogy and potentially problematic minerals, such as expandable clays. All sixteen of the core samples from 35-13 were analyzed by X-ray diffraction methods and prepared as thin sections, and of these, twelve samples were selected for petrographic description.

For the 27-15 well cuttings, X-ray diffraction was conducted on samples collected every 20 ft throughout the 3000-3600 ft depth interval, resulting in a total of thirty-one XRD samples. Of the thirty-one thin sections made, sixteen were selected for further petrographic analysis.

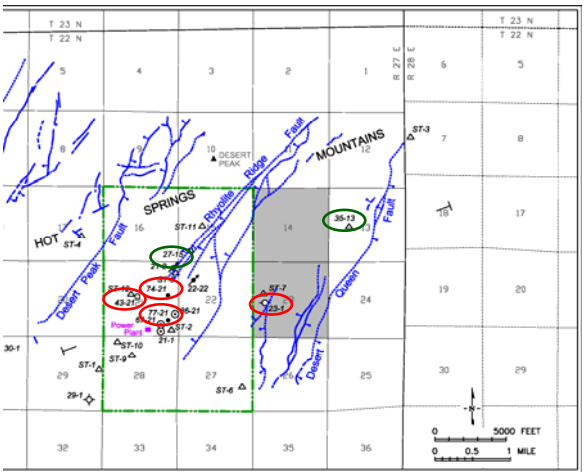

Figure 1: Location of wells in the Desert Peak geothermal field, most of the productive wells are located in Section 21. Wells circled in red represent previously studied wells (Lutz et al., 2009); those circled in green are wells in the current study. Well 27-15 is the planned EGS well. Core samples for the mechanical testing are from Well 35-13. Surface fault traces in blue are based on mapping by Faulds and Garside (2003).

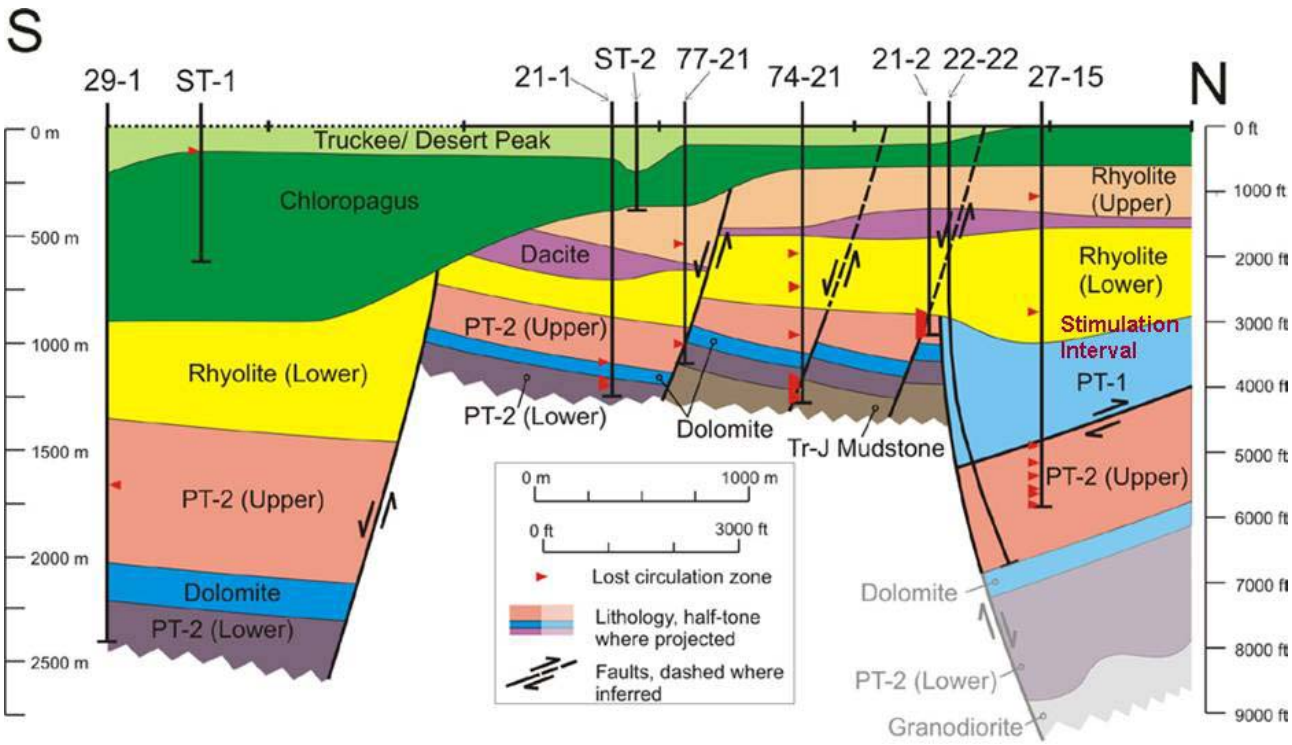

Figure 2: The planned stimulation interval is between 3000 ft and 3500 ft (930-1085 m) in EGS Well 27-15; at the base of Tertiary Rhyolites and at the top of pre-Tertiary metasedimentary rocks (PT1) within the metamorphic basement (modified from Lutz et al., 2009). Wells 22-22 and 21-2 are injection wells; Wells 74-21, 77-21, and 21-1 are active producers.

Rock Mechanical Testing

Mechanical and petrophysical property analyses were conducted on selected core samples collected from Well 35-13. The testing program consisted of:
1) Continuous strength profiling of all rock types within the core segments using TSI™ scratch testing;
2) Drained triaxial compression testing on suites of room temperature vertical samples for Mohr-Coulomb failure envelope delineation with simultaneous ultrasonic velocity measurements; and
3) Basic petrophysical properties (i.e., porosity and permeability at ambient stress conditions).

For this test program, Ormat provided sixteen core sections from various depths within Well 35-13. The purpose of the testing was as follows:
1) To provide an overall assessment of heterogeneity in rock strength using scratch testing (TSI™).
2) To provide strength and rock physics information for developing a failure model for the material. With adequate measurements of strength on core samples, and with the availability of supplementary information such as clay content, sonic velocity and porosity, logging-based predictions of in-situ strength may be possible. With such information, predictions of borehole stability and stress conditions can be performed.
3) To provide static and dynamic mechanical properties that can be used in concert with well logs for predicting reservoir response during hydraulic stimulation and injection/production and for creating 3-D stress models (e.g., Davatzes and Hickman, 2006). Physical/mechanical response of a material is dependent on the rate at which it is loaded and the applied stress/strain amplitude. Logging-based measurements are in the kilohertz range; whereas actual physical loading rates acting on a wellbore and in the reservoir are generally much slower (pseudo-static). We conducted laboratory pseudo-static testing for measurement of Young's modulus (E) and Poisson's ratio (n) while simultaneously measuring dynamic (high loading rate and low loading magnitude) responses of core samples. These parameters provide information for well-log calibration, to provide realistic deformation parameters (E, n) for the engineering and design of hydraulic fracturing and other well stimulation and production activities.

PETROLOGIC DESCRIPTION

In the two study wells, the basic lithologies within the basal part of the rhyolite sequence and at top of the metamorphic basement are similar (Table 1). Three major types of rhyolite tuffs are identified based on the degree of devitrification and type of secondary or hydrothermal alteration: devitrified, argillic, and siliceous. Metamorphic rocks generally consist of two endmember rock types that are gradational in mineralogic composition and in degree of metamorphic foliation, and are classified as either illitic/siliceous metamudstone or siliceous metamudstone.

Table 1. Lithologic Correlation for Rock Mechanics Testing

Well 35-13 Test Sample No.	Well 35-13 Depth Interval (ft)	General Lithotype	Equivalent depth(s) for these lithotypes in Well 27-15 (ft)
ODP1	2286	devitrified rhyolite	3040-3070
ODP2	2376	argillic rhyolite	3000-3030, 3080-3090
ODP3	2392		
ODP4	2437	siliceous rhyolite	3100-3290
ODP5	2483		
ODP6	2579		
ODP12	2591	illitic/siliceous metamudstone	3540-3590
ODP13	2624		
ODP7	2741	siliceous metamudstone	3600-3610

Rhyolite Lithotypes

In less altered rhyolites, relict shard texture with fiamme or flattened pumice fragments clearly identifies ash flow tuffs. Flow-banding in rhyolitic glass and spherulitic devitrification characterize individual tuff units in more strongly welded tuffs. Some of the tuffs contain resorbed and embayed quartz and sanidine crystals, but most of the plagioclase phenocrysts are replaced by fine quartz and clay minerals. Relatively unaltered, *devitrified rhyolite* has about 40% quartz and 20% potassium feldspar, and variable amounts of plagioclase depending upon the original crystal content (up to about 20%) and the extent of plagioclase alteration.

In *argillic rhyolite*, much of the potassium feldspar formed by devitrification of the original volcanic glass is further altered to clay minerals. In Well 27-15, the rhyolite at 3080-3090 ft is argillically-altered and has 32% quartz and 32% total clay; 26% of the whole rock composition consists of illite. In Well 35-13, Samples ODP2 and ODP3 (2376 and 2392 ft) have 36-37% quartz and 31-43% total clay. These samples only have 3-4% potassium feldspar remaining in the strongly clay-altered rhyolite. Well 35-13 is several miles from the main geothermal area (Figure 1) and the corresponding core interval is also about 1000 ft shallower than in Well 27-15, so the clays are less thermally mature. Clay minerals in the core samples from 35-13 are dominated by smectite (5-14%) and smectite-rich illite-smectite (5-11%). In

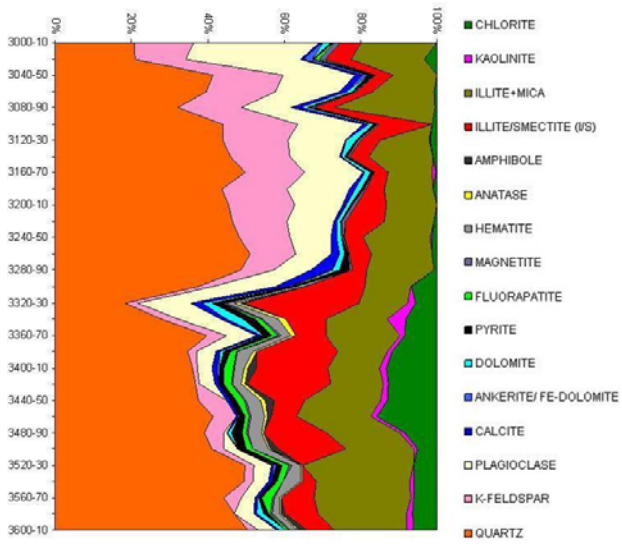

Figure 3: XRD mineralogy of well cuttings samples in the proposed stimulation interval of Well 27-15 (in relative weight percent). The contact between overlying Tertiary rhyolites and the metamorphic basement occurs at a depth of approximately 3300 ft.

Well 27-15, layers of clay alteration along bedding planes are easily identified as highly conductive planar features in Formation Microscanner™ (FMS) images (Kovac et al., 2009).

The most *siliceous rhyolites* are comprised of 40-50% quartz, and are represented at depths of 3100-3280 ft in Well 27-15, and 2437-2530 ft in Well 35-13. In the upper parts of these zones, the rocks are generally dense and non-brecciated. With increasing depth in 27-15, the tuffaceous units are more silicified and have fine quartz veinlets that cut across the rock. In 35-13, most of the rhyolite core samples are densely welded, siliceous tuffs without abundant veins; samples ODP4, 5, and 9 (2437-2530 ft) are especially uniform in overall texture. XRD analyses indicate a rather homogenous composition in this interval with 40-43% quartz, 23-31% potassium feldspar, 8-12% plagioclase, and 16-19% clay.

In Well 27-15, the base of the rhyolite sequence is highly silicified and recrystallized, and original tuffaceous textures are generally obscured. The phyllic hydrothermal alteration assemblage consists of pervasive quartz, potassium feldspar, illite, and pyrite. FMS images in this well exhibit an absence of bedding planes in the 3190-3300 ft interval (Kovac et al., 2009), but the presence of several minor flowing fractures are identified by temperature and spinner flowmeter surveys (Davatzes and Hickman, 2009). In thin section, thicker (0.5 mm) veins are filled with blocky calcite and have just a thin selvage of prismatic quartz crystals. XRD analysis of the 27-15 well cuttings from 3280-3290 ft indicates up to 5% calcite veins and 2% dolomite alteration, as well as 3% pyrite in the silicified rock. Chemical dissolution of these carbonate-filled veins could potentially enhance permeability in these relatively tight siliceous rhyolites (Xu et al, 2009).

Basement Lithologies

The upper part of the basement within the planned stimulation interval of Well 27-15 consists of moderately metamorphosed hematitic mudstones associated with the Jurassic Humboldt Igneous Complex and underlying lower Jurassic and upper Triassic metasediments. In Well 35-13, basement lithologies are more typical of the Pre-Tertiary 1 (PT1) package of weakly metamorphosed siliceous shales, dolomudstones and metatuffs described from other wells to the north and east of the Desert Peak production area (Lutz et al., 2003; 2004; 2009). XRD analysis of the 35-13 core samples indicates a fairly uniform mineralogical composition with 42-55% quartz and 28-42% clay in illitic/siliceous metamudstones. The contact between overlying Tertiary tuffs and the metamorphic basement occurs at about 3300 ft in Well 27-15, and between 2579.8 ft and 2587.0 ft in Well 35-13.

The top of the basement in Well 27-15 (3320-3350 ft) consists of biotite schist and biotite-rich metavolcanic rocks. The cuttings are composed of large folded biotite, quartz, and plagioclase crystals within a highly deformed chloritic and hematitic matrix. In XRD (Figure 3), the increase in overall chlorite content (from 1-2% in the rhyolite, up to 6-16% in deeper samples) is an indication that metamorphic rocks in the basement have been transected by the well. Iron and titanium oxide mineralization consists of magnetite (1%), hematite (2-4%), and anatase (2%).

Below 3360 ft in Well 27-15, the metamorphic rocks are less deformed and more fine-grained and siliceous, but are still strongly mineralized with hematite. Between 3360 ft and 3480 ft, the rocks are fairly massive hematitic mudstones composed of 35-40% quartz, less than 10% feldspar, up to 4% hematite, 37-50% total clay, and with trace amounts of carbonate and amphibole minerals. At 3480-3520 ft, the hematitic mudstones exhibit some fault gouge development in the cuttings, and there is a lithologic change to more siliceous and pyritic mudstones below. These siliceous mudstones are composed of up to 50% quartz and 34% illitic clay. The cutting samples from 3520 to 3600 ft are generally more foliated than the overlying hematitic mudstones. Aligned muscovite plates and finely crystalline illite exhibit weak to moderate foliation in these pelitic rocks.

Thrust faults and other Mesozoic-aged faults complicate the basement stratigraphy. The FMS images show strong foliation in the metamudstones

and dramatic changes in foliation orientations across formation contacts, indicating extensive folding or faulting in this section of the well (Kovac et al., 2009). Temperature and spinner flowmeter surveys reveal the presence of relatively permeable fractures that are well oriented for normal faulting, in addition to fluid flow that is preferentially developed along formation boundaries (Davatzes and Hickman, 2009; Hickman and Davatzes, 2010).

PETROLOGIC EFFECTS ON MECHANICAL CHARACTER

Texture and Strength

Laboratory testing of the Well 35-13 core samples reveals variable strengths and a range of other mechanical properties for the different lithologies. In the rhyolites, the character of the tuffaceous matrix controls the overall mechanical characteristics of the rock. In the basement rocks, the degree of metamorphic foliation and the fracturing intensity controls the mechanical behavior.

Overall, the evaluated rhyolite samples exhibit high porosity but poor permeability within the devitrified and microporous tuffaceous matrices (Table 2). In the meta-sedimentary rocks, the dense siliceous matrix is less porous, and open fractures are the dominant pore type. Mineralogic and textural characteristics revealed by the petrologic analyses have strong effects on the mechanical behavior. These characteristics are discussed below:

- Matrix Composition – This is likely the single most important control on overall rock strength. Whether the rock is a siliceous rhyolite or a siliceous metasedimentary rock, it is the quartz content in the matrix that cements the matrix and supports the rock under a variety of confining pressures. Results of the triaxial testing indicate that the most siliceous rhyolites and metasedimentary rocks have the highest rock cohesion and overall strength (Tables 3 and 4). In contrast, the devitrified and argillaceous rhyolites with abundant potassium feldspar and smectite-rich illite-smectite in the matrix exhibit lower rock strengths.
- Matrix Fabric – In the rhyolites, silicification and pervasive spherulitic devitrification is associated with higher cohesive strengths (Table 4) presumably because the spherules inhibit compaction and the formation of clayey laminae that could act as planes of weakness under compressive stress. The rounded spherule morphology should absorb stress, increase contact surface areas, and limit grain-scale microcracking and cataclastic pore collapse. The matrix in these dense silicified units is typically massive or homogeneous without well-defined bedding breaks. Where larger pumice fragments are compressed and flattened along bedding planes, or where the ash flow tuffs are more clay-altered or flow-banded, matrix microtexture is more heterogeneous and could be more prone to cataclasis and pore compaction.
- In the metamorphic rocks, pre-existing foliation planes, mineralogical differentiation, and older intersecting veins create a network of planar features with aligned and segregated micas, illitic clays, and other weak phyllosilicates that are more likely to fail under relatively low shear stress than more homogenous rocks with a more random microstructure.
- Crystal and Clast Content – The ash flow tuffs are generally crystal-poor, but there are great contrasts in strength and other elastic properties between the microporous ashy matrix and adjacent blocky plagioclase and quartz phenocrysts. As in tuff agglomerates or conglomerates, failure planes typically wrap around harder clasts or crystals in the core plugs (e.g., Figure 5 below). Although the metamorphic rocks are well cemented, the volcaniclastic metamudstones have similar large clasts embedded in a fine matrix, creating strength heterogeneities in these rocks as well.
- Ductile Grains and Clays - Comparatively soft detrital components such as tuffaceous particles, dissolved or devitrified volcanic rock fragments, biotite and other detrital or metamorphic micas, as well as authigenic clays are abundant in both the volcanic and metasedimentary rocks. Authigenic kaolinite and illite-smectite clays are especially abundant in the matrix of the tuffaceous rocks. These clays could lead to increasing compressibility in the more argillaceous rhyolites, and ductile deformation or clay smearing during shear failure (see Figure 5). The type of clay also affects the mechanical character; in that smectite-rich clays are weaker and smear more easily than illite or chlorite clays (Lockner and Beeler, 2002).
- Vein Mineralogy and Fracture Intensity - In the rhyolites, densely silicified rocks along the basement contact have crosscutting fine quartz veinlets. These are mostly sealed and probably help support the rocks against compressive stress, but a few of the larger veins are filled with poorly cohesive late-stage calcite or have minor open fracture porosity in the centers of the quartz veins. The latter could act as planes of weakness, and if hydraulically stimulated could increase permeability in these tight rocks.

  The metamorphic rocks are fractured, especially along the previously eroded top of the basement,

and possibly along older faults between different metasedimentary packages. In Well 35-13, some of the fractures are filled with low temperature carbonates (siderite, dolomite, calcite) and barite, but many of the core pieces have extensive open fractures. The mechanical tests were conducted on the least fractured core pieces, but these also show failure planes along pre-existing planar features such as older veins.

- Primary/Secondary Porosity – The devitrified and argillaceous rhyolites are much more porous and permeable than the siliceous tuffs. The porosity is dominated by matrix micropores between very finely crystalline quartz, potassium feldspar, and clay particles in the devitrified matrix. Devitrification spherules are especially permeable because the rock matrix is not compacted and the micropores are well-connected in a radial pattern between the fine crystallites. In the dense siliceous rhyolites, the matrix is cemented by clots of quartz crystals and quartz-replaced pumice fragments, and permeability values are much lower (Table 2). Many of the matrix micropores are also clogged with authigenic kaolinite and clayey or cherty pseudomatrix. The porous and permeable devitrified and argillaceous rhyolites have less silica to support the rock framework and exhibit lower intact rock strengths than the more siliceous rhyolites (Table 4).

RESULTS OF MECHANICAL TESTING

Triaxial compression tests were conducted on cores from Well 35-13 using a servo-controlled testing apparatus which subjected the samples to the desired stress states at controlled strain rates. Prior to testing, each test sample was placed between two end-caps and jacketed with either a Teflon® or polyolefin sleeve. The jacketed test specimen was then instrumented with axial and radial cantilevers for strain measurement and installed in the pressure vessel for testing.

For failure characterization, suites of single-stage triaxial compression tests were conducted on vertical samples (i.e., samples aligned parallel to the borehole axis) in order to construct Mohr stress circles and calculate Coulomb parameters for both peak compressive strength corresponding to initial failure of the intact rock, and residual effective compressive strength corresponding to quasi-stable frictional sliding on the newly formed fracture at the end of each test. Triaxial compression tests were performed with air as the pore fluid and pore pressure drained to the atmosphere. Results of triaxial compression tests and residual strengths, including quasi-static mechanical properties, are summarized for the three most dominant lithologies in Table 3. Summary plots for the failure characterization in devitrified versus siliceous rhyolites are shown in Figure 4.

Dynamic mechanical properties using ultrasonic wave transmission (with 1MHz P- and S-wave transducers) were determined concurrently with all triaxial compression tests. Ultrasonic velocities and dynamic mechanical properties (Young's modulus and Poisson's ratio) were also determined for the 35-13 core samples (Table 3).

Scratch tests were also conducted along the length of the core segments using TSI™ scratch testing apparatus to provide semi-quantitative, empirical information on variations in unconfined compressive strength with lithology and extent of veining. More details on all the tests conducted on the core samples from Well 35-13 can be found in TerraTek Report TR09-402855 (TerraTek, 2009).

SUMMARY OF MECHANICAL PROPERTIES BY LITHOTYPE

The following tables list representative test results from the routine core analyses, uniaxial or unconfined compression stress tests (UCS) from the TSI™ scratch testing, triaxial compression tests, and Mohr-Coulomb failure evaluations for general lithotypes within the studied interval of Well 35-13. Table 2 presents porosity and permeability relationships for selected samples, and Tables 3 and 4 represent a summary of the scratch testing and triaxial compression test results along with derived parameters for the Mohr-Coulomb failure envelopes.

In Table 4, the internal friction angles and internal linear cohesions are calculated by fitting a tangential line to the population of Mohr circles defined at the peak axial stresses at initial failure for each confining pressure (the red circles in Figure 4). The residual friction angles and residual cohesions represent the tangents to Mohr circles defined from the final, quasi-stable axial stress at initial failure for each confining pressure (the green circles in Figure 4). These residual friction angles, φ, are used to determine the coefficients of sliding friction, μ from the expression $\mu = \tan \varphi$. Hickman and Davatzes (2010) use these sliding friction values in concert with two end-member 3-D stress models to determine the propensity for frictional failure along fractures seen in the stimulation interval from Well 27-15 as a function of excess fluid pressure. These calculations are being used to design optimal injection parameters for hydraulic stimulation during the Desert Peak EGS project. Note that the residual cohesions shown in Table 4 are likely an artifact of the finite strength of the jackets used to enclose these samples during testing, and thus should be neglected when calculating actual sliding friction on pre-fractured rock.

Based on the results of compression strength testing at a series of confining pressures (1, 4, 10, and 20 MPa), the stiffer siliceous rhyolites display moderately high Young's modulus values (Table 3). Although the metasedimentary rocks were tested at only two confining pressures (4 and 10 or 20 MPa) and the material properties are less well constrained, these siliceous rocks also display high Young's moduli. The strongest rocks in the sample suite appear to be the unfractured or minimally veined siliceous rhyolites and siliceous metamudstones, although the metamorphic rocks generally have higher peak and residual cohesive strengths than the rhyolites (Table 4). Quasi-static values for Young's modulus and Poisson's ratio ranged from 6538 MPa (in argillaceous rhyolite) to 41,700 MPa (in siliceous metamudstone), and 0.08 to 0.24, respectively (TerraTek, 2009). The greatest increase of Young's modulus values with increasing confining pressures occurs within argillic rhyolite. For example, for Sample ODP2 at 2376 ft, Young's modulus is 6806 MPa at an effective confining pressure of 1 MPa; whereas at 10 MPa, it is 17,920 MPa (TerraTek, 2009). These weaker argillaceous rocks start out at low values of Young's modulus and then appear to compact (become stiffer) at higher confining pressures, thereby increasing Young's modulus. Such an effect is not seen in the already well-cemented siliceous rocks.

Comparison of these data sets indicates overall moderate rock strengths; with UCS estimates from TSI™ testing of about 17,000-27,000 psi (117-186 MPa) for the more siliceous lithologies, and about 12,000-16,000 psi (82-110 MPa) for the argillaceous and devitrified rhyolites (Table 4). The devitrified and argillaceous rhyolites and illitic metasedimentary rocks have the highest initial porosities, with up to 21% porosity recorded for the devitrified rhyolites (Table 2). Comparison of somewhat spotty pre- and post-test core data appears to indicate up to a 20-fold increase in permeability as a result of dilational failure in originally tight (<5% porosity) argillaceous rocks. However, the methods used to determine permeability on the jacketed post-test core plugs can not distinguish gas flow through the rock from flow around the outside of the fractured sample. The magnitude of the permeability increase may be difficult to measure, but certainly the core test plugs have undergone dilation and brittle failure, and large aperture fractures are observed in the post-failure CT-scans (Figure 5), bolstering the high pre- versus post-test permeability ratios.

Table 2. Pre- and Post-Test Porosity and Permeability Relationships

Well 35-13 Test Sample and Depth	General Lithotype	Pre-Test Ambient Porosity (%)	Pre-Test Gas Perm (md)	Post-Test (2900 psi, 20MPa) Gas Perm (md)*	Post-Test Perm/ Pre-Test Perm
ODP1 2286 ft	devitrified rhyolite	20.72	0.013	0.149	11.462
ODP2 2376 ft	argillic rhyolite	11.44	0.375	0.042	0.112
ODP3 2392 ft		4.61	0.020	0.398	19.900
ODP4 2437 ft	siliceous rhyolite	8.71	<0.001	10.295	n.a.
ODP5 2483 ft		8.28	0.003	0.022	7.333
ODP6 2579 ft		12.99	<0.001	0.122	n.a.
ODP12 2591 ft	illitic/siliceous metamudstone	9.08	-	42.093	-
ODP13 2624 ft		11.89	-	0.873	-
ODP7 2741 ft	siliceous metamudstone	4.66	-	2.171	-
ODP16 2742		0.96	11.427	-	-

*Post-test permeability conducted on teflon-jacketed fractured core plugs

Table 3. Summary of Triaxial Compression Tests for Selected Samples - Desert Peak 35-13

Depth and General Lithotype	Sample ID	As-Received Bulk Density (g/cm^3)	Effective Confining Pressure[1] (MPa)	Effective Compressive Strength (MPa)	Residual Effective Compressive Strength (MPa)	Quasi-Static Young's Modulus (MPa)	Quasi-Static Poisson's Ratio
2286 ft devitrified rhyolite	ODP1-2	2.120	1	52.28	17.1	8510	0.15
	ODP1-5	2.086	4	55.43	26.7	6538	0.14
	ODP1-1	2.107	10	78.85	51.4	7819	0.17
	ODP1-4	2.106	20	105.04	81.3	8216	0.21
2437 ft siliceous rhyolite	ODP4-3	2.406	1	108.17	16.4	22,100	0.13
	ODP4-2	2.407	4	138.15	36.7	25,410	0.18
	ODP4-1	2.410	10	170.83	56.3	25,970	0.18
	ODP4-5	2.419	20	227.29	104.8	26,490	0.19
2624 ft illitic/siliceous metamudstone	ODP13-2	2.711	4	132.31	47.6	30,340	0.40
	ODP13-1	2.719	20	213.68	127.9	38,090	0.17

[1] Pore pressure = 0 psi in all tests

Table 4. Calculated Unconfined Compressive Strength (UCS) and Mohr-Coulomb Properties

Well 35-13 Test Sample and Average Depth	General Lithotype	Average UCS (as calculated from TSI™ tests)		Mohr-Coulomb Properties				
		(psi)	(MPa)	Internal Friction Angle (degrees)	Internal Linear Cohesion (MPa)	Residual Linear Cohesion (MPa)	Residual Friction Angle (degrees)	Coefficient of Sliding Friction (μ)
ODP1 2286 ft	devitrified rhyolite	12,000	82.8	29.3	13.84	3.82	33.3	0.655
ODP2 2376 ft	argillic rhyolite	16,000	110.3	35.4	10.02	3.63	35.2	0.704
ODP3 2392 ft		15,000	103.4	32.5	12.85	4.38	33.0	0.650
ODP4 2437 ft	siliceous rhyolite	26,000	179.3	45.9	21.86	3.31	39.6	0.827
ODP5 2483 ft		19,000	131.0	38.2	24.02	1.74	40.5	0.855
ODP6 2579 ft		17,000	117.2	47.6	19.23	0	43.9	0.962
ODP12 2591ft	illitic/siliceous metamudstone	21,100	144.8	44.4	12.75	1.93	50.5	1.215
ODP13 2624ft		27,000	186.2	42.2	24.83	6.13	41.9	0.898
ODP7 2741 ft	siliceous metamudstone	26,000	179.3	33.8	34.89	13.27	33.6	0.664

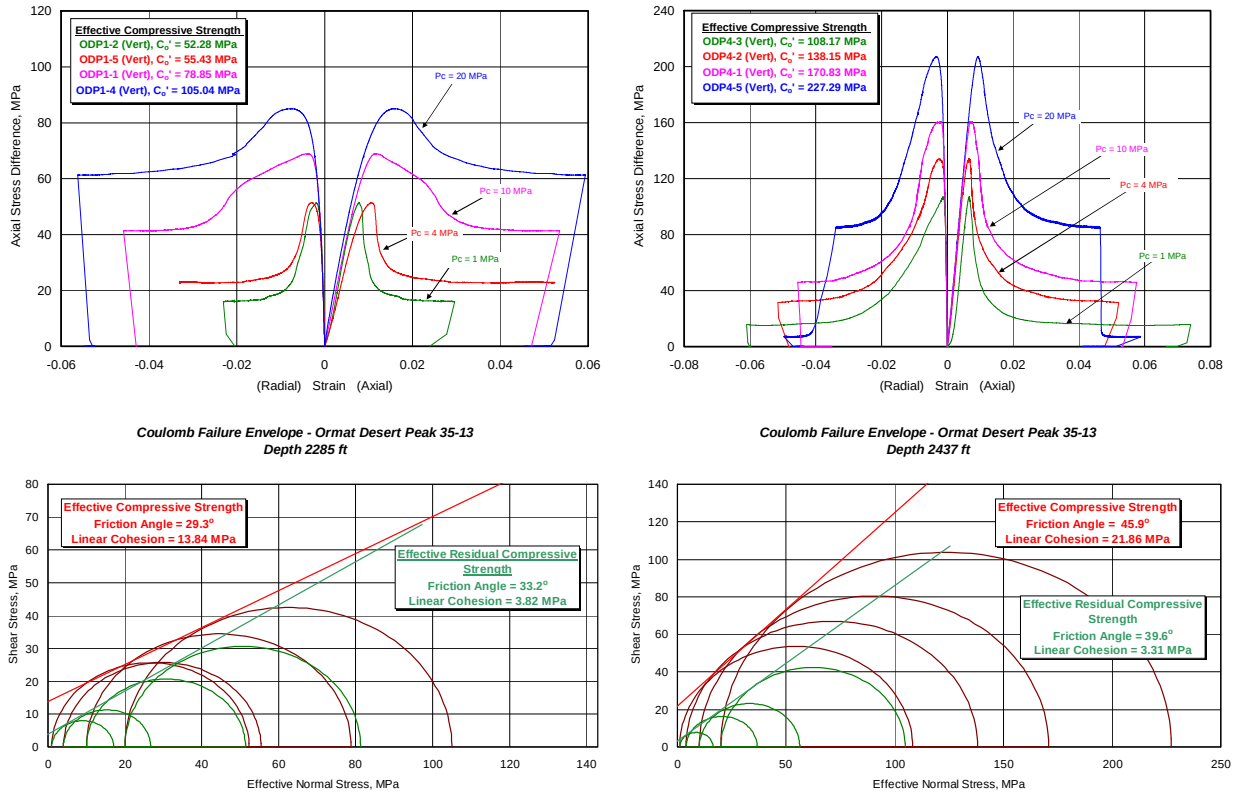

Figure 4. Comparison of failure behavior between devitrified, less stiff rhyolite at 2285 ft (left), and stonger, more siliceous rhyolite at 2437 ft (right). The upper plots show the results of triaxial compressive tests and the stress-strain response for four vertical samples under confining pressures of 1, 4, 10 and 20 MPa. The effective compressive strength is indicated for each test. The lower plots present Coulomb failure envelopes for the four vertical samples from each depth. Coulomb criteria (friction angle and linear cohesion) were determined for two ranges – peak effective compressive strength (red) and effective residual compressive strength (green) for the entire test group. High residual cohesions are likely an effect of the plastic jackets on the fractured core plugs.

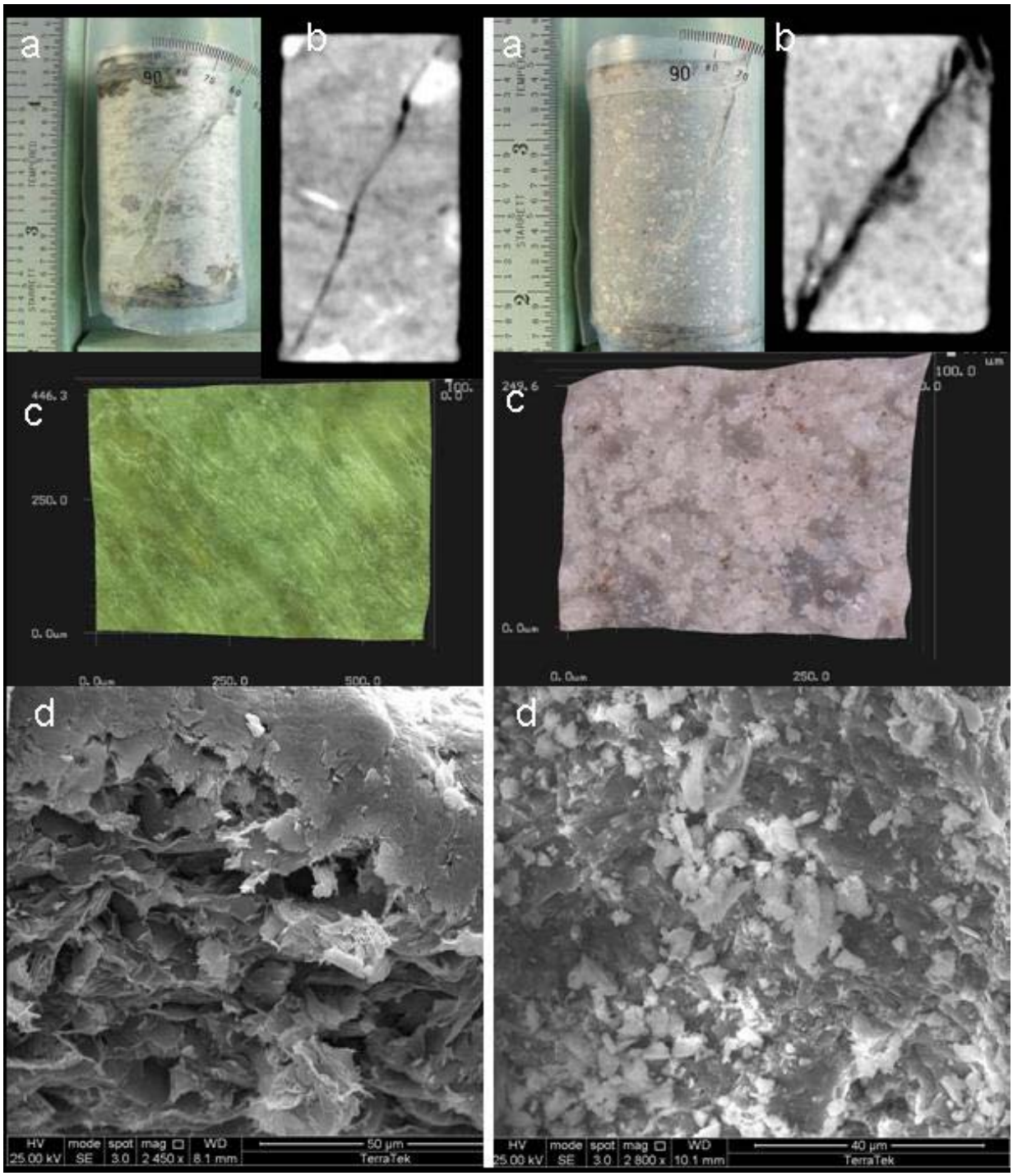

Figure 5. Multiple scales of observation of induced failure planes produced during triaxial compression testing (conducted at confining pressures of 4MPa, similar to conditions at the proposed stimulation depths within Well 27-15): a) jacketed post-test, fractured core plugs; b) CAT-scan images of these same core plugs, c) 3-D profiling microscopy of the developed fracture planes, and d) scanning electron microscope images of the failure surfaces. The images on the left represent devitrified rhyolite tuff (Sample ODP1) and show a curved fracture plane (b), well-developed slickensides in clayey material along the failure plane (c), and smeared clay over the highly microporous argillaceous matrix (d). The images to the right represent dense siliceous rhyolite tuff (Sample ODP4) that broke into several straight fractures (b), and produced abundant quartz-rich rock flour (c and d) that could act to self-prop the newly created fracture within the tight matrix.

CONCLUSIONS

Most of the rocks in the proposed stimulation interval within Well 27-15 are moderately siliceous, fine-grained rocks. The clay content of the rhyolitic rocks and metamorphic mudstones is also moderately high and it is the clay mineralogy that controls the porosity and texture of the matrix materials, while the siliceous mineralogy supports the matrix and increases overall rock strength. The results of the mechanical testing indicate that these rocks are generally good candidates for hydraulic stimulation. Other factors that may affect their behavior during chemical or mechanical stimulation include heterogeneity related to veins, fractures, texture, temperature, pore pressures, and in-situ and tectonic stresses. Preliminary scanning electron microscopic (SEM) examination of the induced failure planes created during these mechanical tests indicates that smectite-rich clays in the argillaceous rhyolites may deform ductilely under higher stress conditions. Thus. these planes lined with low cohesion clayey materials may act as planes of weakness to localize shearing during stimulation but are not expected to create significant, dilatant permeability in the rock. In contrast, brittle deformation in the more siliceous rocks is characterized by the production of quartz-rich rock flour that may act as a proppant, preserving permeability along newly formed fractures after the hydraulic stimulation has ceased. This interpretation is supported by high measured permeability gains and observations of significant residual fracture porosity in these rocks following shearing.

Coulomb failure calculations assuming cohesionless pre-existing fractures with coefficients of friction of 0.6 or higher (consistent with the results of these core tests) indicate that shear failure could be induced on well-oriented fractures seen in Well 27-15 once fluid pressures are increased above the ambient formation fluid pressure (Hickman and Davatzes, 2010). This geomechanical model will be tested during hydraulic stimulation of well 27-15 as part of the Desert Peak EGS Project, which is intended to enhance formation permeability through self-propping shear failure.

Acknowledgements

The Desert Peak EGS project is supported by the U.S. Department of Energy, Assistant Secretary for Energy Efficiency and Renewable Energy, under DOE Grant No. DE-FC36-02ID14406.

REFERENCES

Davatzes, N.C. and S. Hickman, 2006, Stress and faulting in the Coso Geothermal Field: Update and recent results from the East Flank and Coso Wash: Proceedings, Thirty-First Workshop on Geothermal Reservoir Engineering, Stanford University, Stanford California, January 30-February 1, 2006 SGP-TR-179.

Davatzes, N., and Hickman, S., 2009, Fractures, stress, and fluid flow prior to stimulation of Well 27-15, Desert Peak, Nevada, EGS Project: Proceedings, Thirty-Fourth Workshop on Geothermal Reservoir Engineering Stanford University, Stanford, California, February 9-11, 2009 SGP-TR-187.

Faulds, J.E., and Garside, L.J., 2003, Preliminary geologic map of the Desert Peak – Brady geothermal fields, Churchill County, Nevada: Nevada Bureau of Mines and Geology Open-File Report 03-27.

Faulds, J.E., Garside, L., and Oppliger, G.L., 2003, Structural analysis of the Desert Peak-Brady Geothermal Fields, northwestern Nevada: Implications for understanding linkages between northeast-trending structures and geothermal reservoirs in the Humboldt structural zone: Geothermal Resources Council Transactions, v. 27, p. 859-864.

Hickman, S., and Davatzes, N., 2010, In-situ stress and fracture characterization for planning of an EGS stimulation in the Desert Peak geothermal field, NV: Proceedings, Thirty-fifth Workshop on Geothermal Reservoir Engineering Stanford University, Stanford, California, February 1-3, 2010 SGP-TR-188.

Kovac, K., Lutz, S.J., Drakos, P. S., and Robertson-Tait, A., 2009, Borehole image analysis and geological interpretation of selected features in Well DP 27-15 at Desert Peak, Nevada: Pre-stimulation evaluation of an Enhanced Geothermal System: Proceedings, Thirty-Fourth Workshop on Geothermal Reservoir Engineering Stanford University, Stanford, California, February 9-11, 2009 SGP-TR-187.

Lockner, D.A., and N.M. Beeler, 2002, Chapter 32, in International Handbook of Earthquake and Engineering Seismology , edited by W.H.K. Lee, H. Kanamori, P.C. Jennings, and C. Kisslinger, Academic Press, Amsterdam, pp. 505-537.

Lutz, S.J., A. Schriener Jr., D. Schochet and A. Robertson-Tait, 2003. Geologic characterization of pre-Tertiary rocks at the Desert Peak East EGS project site, Churchill County, Nevada. Transactions, Geothermal Resources Council, Vol. 27, pp.865-870.

Lutz, S.J., Robertson-Tait, A., and Morris, C.L., 2004, Stratigraphic relationships in Mesozoic basement rocks at the Desert Peak East EGS area, Nevada: Proceedings, Twenty-Ninth Workshop on Geothermal Reservoir Engineering Stanford University, Stanford, California, January 26-28, 2004 SGP-TR-175.

Lutz, S.J., Moore, J.N., Jones, C.G., Suemnicht, G., and Robertson-Tait, A., 2009, Geological and structural relationships in the Desert Peak geothermal system, Nevada: Implications for EGS development: Proceedings, Thirty-fourth Workshop on Geothermal Reservoir Engineering Stanford University, Stanford, California, February 9-11, 2009 SGP-TR-187.

TerraTek, 2009, Failure and Physical Characterization of Selected Materials: Desert Peak 35-13, *Technical Report TR09-402855* prepared for Ormat Nevada, November 2009, TerraTek- A Schlumberger Company, Salt Lake City, UT.

Xu, T., Rose, P., Fayer, S. and Pruess, K., 2009, Numerical simulation study of silica and calcite dissolution around geothermal wells by injecting high pH solutions with chelating agent: Proceedings, Thirty-fourth Workshop on Geothermal Reservoir Engineering Stanford University, Stanford, California, February 9-11, 2009 SGP-TR-187.